Response to Reviewers

Dear editor and reviewers:

Thank you very much for your letter and the constructive comments concerning our manuscript, entitled "*Impacts of synoptic circulation types on nocturnal ozone increase in the North China Plain: Meteorological drivers and physical mechanisms*" (Manuscript ID: egusphere-2026-25).

We deeply appreciate the time and effort you have dedicated to reviewing our work. The insightful feedback has been exceedingly valuable in refining our terminology, strengthening our scientific arguments, and improving the overall quality of the paper. We have carefully considered all the comments and revised the manuscript accordingly.

Please find below our detailed point-by-point responses to the specific comments as follows:

Reviewers' comments are in black.

Authors' responses are in blue.

Changes in the manuscript are in red.

Your Sincerely,

Liya Fan,

On behalf of the authors

Reviewer #3

1. Introduction: The framing around the need to study nocturnal NOI — as opposed to daytime ozone, which is better characterized — has become repetitive. The argument is made multiple times and should be consolidated into a single, concise statement.

Response 1: Thanks for reviewer's comments. We have removed the repetitive argument and consolidated the argument into a single and concise statement.

Lines 65-67:

However, while the synoptic and meteorological drivers of daytime photochemical O_3 are well-established, their specific dynamic roles in governing nighttime NOI remain underexplored, particularly in rapidly urbanizing regions like the NCP.

2. Introduction: Figure S1 needs significant improvement. The map is of poor quality, the figure title does not describe what is shown, and the use of station acronyms without explanation is unhelpful for an international reader. S1 does not succeed in contextualizing the problem geographically or in terms of emission environment taking into consideration what has been described in the introduction.

Response 2: Thanks for reviewer's comments. We have redesigned and redrawn Figure S1.

Figure S1:

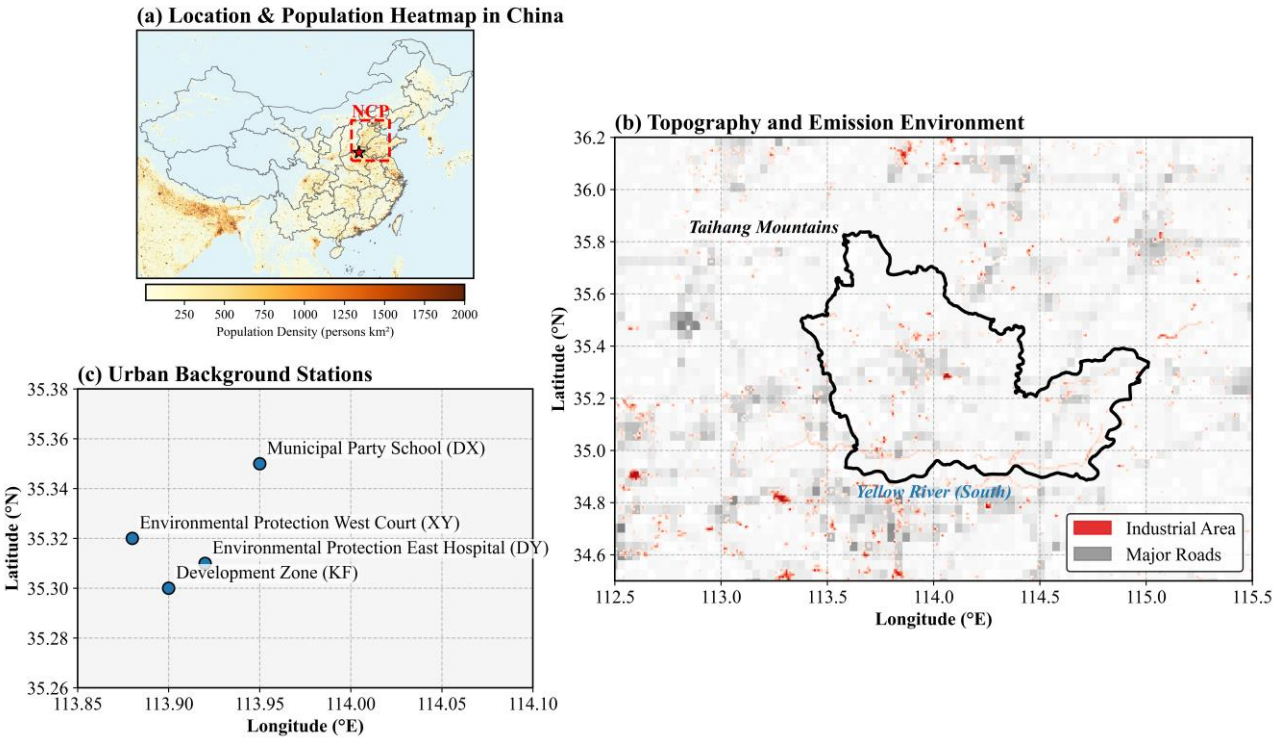


Figure S1: Geographical setting, regional emission context, and spatial distribution of monitoring stations. (a) Location of the study area within China, superimposed on the gridded population density distribution. The red dashed rectangle delineates the North China Plain (NCP), and the red star marks the geographical location of Xinxiang. (b) Multi-source emission environment across Xinxiang. Spatial layers depict major industrial area (red) and major roads (dark grey), with the black solid boundary indicating the municipal boundary of Xinxiang. (c) Spatial arrangement of the national air quality monitoring stations (KF (Development Zone), DY (Environmental Protection East Hospital), XY (Environmental Protection West Court), and DX (Municipal Party School)) located in the urban core of Xinxiang. The spatial distribution data for population density, industrial areas, and major roads are derived from Wang et al. (2024a).

3. Introduction: The issue raised in the previous review persists: the location and nature of major emission sources in the region are still not described. Now the four stations are clear to be urban and of broadly similar characteristics.

Response 3: Thanks for reviewer's comments. We have revised and improved Figure S1 to illustrate the location and nature of major emission sources. Furthermore, we have updated the relevant text within the Introduction.

Lines 68-75:

Located in the southern NCP, Xinxiang is bordered by the Taihang Mountains to the north and the Yellow River to the south (Fig. S1(a)). As a densely populated urban center, Xinxiang features a typical temperate continental monsoon climate, characterized by hot, humid summers and cold, dry winters. Furthermore, serving as a major industrial and transportation hub, the city experiences intense anthropogenic emissions. As shown in Fig. S1(b), the primary precursors for O_3 (i.e., NO_x and VOCs) predominantly originate from industrial facilities (e.g., chemical and manufacturing plants) that are densely distributed across the surrounding suburban areas, and intense vehicular exhaust along a highly interconnected network of major transportation arteries traversing the region. These multi-source regional emissions enclose the urban core, exerting a profound influence on the atmospheric chemistry at the four urban background stations (Fig. S1(c)).

4. Methodology: The use of both MERRA-2 and ERA5 needs to be more clearly articulated. When calculations are performed, it should be explicit which reanalysis is used for each variable — specifically, ERA5 at 850 hPa and MERRA-2 from 1000 to 500 hPa. What is reanalysis used for the Lamb-Jenkinson classification? I believe that is MERRA-2, but I encourage to be always explicit with the database used.

Response 4: Thanks for reviewer's comments. We have now clearly articulated the use of both MERRA-2 and ERA5. Specifically, we have stated that the Sea Level Pressure (SLP) data derived from the MERRA-2 dataset was used to drive the Lamb-Jenkinson synoptic weather classification. Furthermore, MERRA-2 was employed for the vertical profiles from 1000 to 500 hPa, while ERA5 was used for the specific humidity (850 hPa) and other boundary layer parameters (e.g., PBLH, U^*, CAPE).

Lines 96-110:

Sea level pressure (SLP) data and 17-layer vertical profiles (500-1000 hPa) of vorticity, wind speed (WS), wind direction, temperature (T), relative humidity (RH) and O_3 concentration were acquired from the Modern-Era Retrospective Analysis for Research and Applications dataset (MERRA-2, Version 2, with a spatial resolution of 0.5° × 0.625° and temporal resolutions of 1 hour for surface data and 3 hours for 3D vertical profiles) (https://disc.gsfc.nasa.gov/). Specifically, the

SLP data from MERRA-2 was used to perform the Lamb-Jenkinson synoptic weather classification. This dataset was constructed by NASA Global Modeling and Assimilation Office (GMAO) using the Goddard Earth Observing System (GEOS) assimilation model, and has been widely applied in weather typing studies worldwide (Zhang et al., 2022; Gelaro et al., 2017; Molod et al., 2015; Li et al., 2020). Additionally, specific humidity (850hpa), planetary boundary layer height (PBLH), friction velocity (U^*), and convective available potential energy (CAPE) were derived from the ERA5 reanalysis dataset (https://www.ecmwf.int/en/forecasts/dataset/ecmwf-reanalysis-v5) (with a spatial resolution of 0.25° × 0.25° and an hourly temporal resolution) provided by the European Centre for Medium-Range Weather Forecasts (ECMWF), which offers superior boundary layer parameters (Hersbach et al., 2020; Bell et al., 2021). Throughout the subsequent calculations, MERRA-2 was consistently employed for the 1000 to 500 hPa vertical profiling, while ERA5 was dedicated to the specific 850 hPa humidity and boundary layer meteorological parameters (e.g., PBLH, U^*, CAPE).

5. Methodology: The NOI identification method still lacks clarity. As currently described, a single 10 μg/m³ increase at a single station in a single hour appears sufficient to flag an event? After this, the calculation or classification is applied based on hourly or daily average? This needs to be explicitly stated.

Response 5: Thanks for reviewer's comments. Yes, consistent with the widely adopted definitions in current literature (e.g., He et al., 2021; Zhu et al., 2020), an hourly O_3 concentration increment exceeding 10 μg m^{-3} at a single monitoring station is sufficient to flag a local NOI event. We have clarified this wording in the manuscript to avoid any ambiguity.

We do not use daily average results for our subsequent analyses, as doing so would dilute the nocturnal dynamic signals with daytime meteorological variations. Instead, all subsequent calculations and classifications are strictly based on the nighttime average results (e.g., averaged over the 20:00-06:00 LT window) corresponding to the identified NOI events.

Lines 116-117:

Specifically, an NOI event is flagged when a single monitoring station records an hourly O_3 concentration increment exceeding 10 μg m^{-3} during nighttime (20:00-06:00 local time, LT; UTC+8,

Beijing Time) (He et al., 2021; Zhu et al., 2020).

Lines 132-136:

Furthermore, to accurately characterize the specific atmospheric background driving these nighttime intrusions, it is important to note that the subsequent calculations and classifications are not based on daily average results. Instead, we strictly used the nighttime average fields (i.e., averaged over the continuous nocturnal window) corresponding to the identified NOI events. This temporal matching effectively prevented the transient nocturnal dynamic signals from being diluted by daytime meteorological variations.

6. Results: Lines 185 onwards: the claim about summer peak activity seems to rest on data from a single station. Do the other stations not show a stronger signal towards autumn? It is hard to agree with the "summer transition" based on NOI.

Response 6: Thanks for reviewer's comments. We have removed the speculative claims and mechanistic explanations regarding the "summer peak / summer transition".

7. Results: Figure S3: the meaning of "WN" is not defined. Does it indicate events occurring both before and after midnight?

Response 7: Thanks for reviewer's comments. "WN" (Whole-night NOI) indicates events that occur across both the pre-midnight (Early-night) and post-midnight (Late-night) periods, persisting continuously through the night. We have added the definitions of WN, as well as EN and LN, into the caption of Figure S3.

Figure S3:

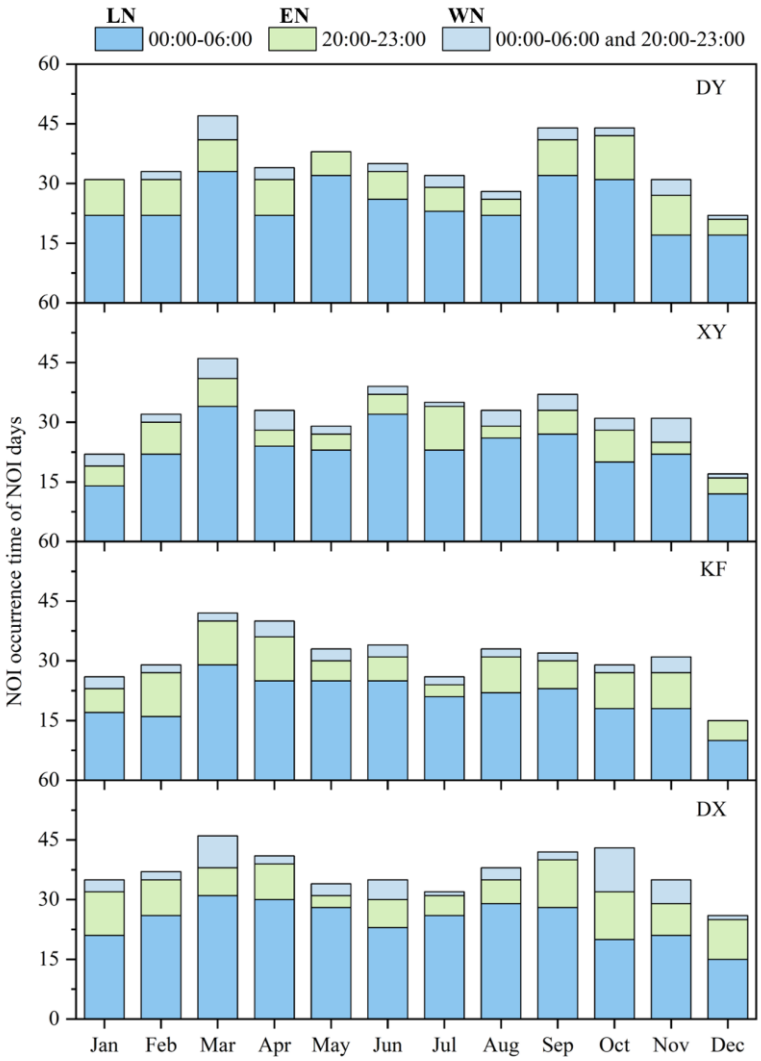


Figure S3: Monthly variation of NOI occurrence time at national monitoring stations in Xinxiang, 2021-2023. The abbreviations (EN, LN and WN) represent three distinct temporal categories of NOI days: Early-night (EN, 20:00-23:00 LT), Late-night (LN, 00:00-06:00 LT), and Whole-night (WN, events persisting continuously across both EN and LN periods).

8. Results: Figure 2 would benefit from consistent scales across panels. The analysis of this figure is very limited given the information it contains — there are interesting features including near-stable values and night peaks that are not discussed. The statistical significance of the mean profiles shown is not reported, and the number of occurrences underlying each composite is not indicated.

Response 8: Thanks for reviewer's comments. We have replotted Figure 2. All panels now share a consistent y-axis scale (0-180 μg m^{-3}). The specific number of occurrences (N) underlying each composite profile has been added to the figure legend. To visually represent the statistical

robustness and variance of the mean profiles, we have added shaded error bands representing ± 1 standard error of the mean (SEM) to all curves in Figure 2.

Additionally, we have expanded the analysis in the text to discuss these anomalous features (near-stable values and night peaks).

Figure 2:

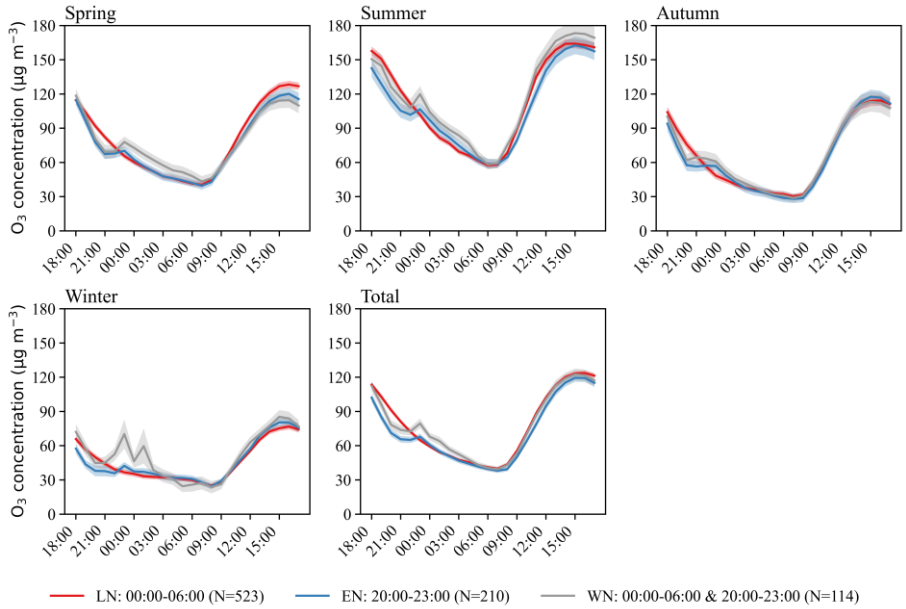


Figure 2: O_3 diurnal variations of NOI days under different NOI occurrence time in different seasons. The solid colored lines represent the composite mean O_3 concentrations for LN (red), EN (blue), and WN (grey). The shaded bands denote the bounds of ± 1 standard error of the mean (SEM), visualizing the statistical variance. The number of occurrences (N) for each specific category is indicated in the legend.

Lines 216-228:

Unlike the typical continuous depletion observed on non-NOI event nights, WN frequently exhibited anomalous night peaks or maintained near-stable, elevated concentrations throughout the dark hours. These features directly reflect the continuous and intense nature of the dynamical intrusions during WN periods, which effectively offset the local chemical depletion (NO titration). In contrast, in spring and summer, LN consistently showed both higher nocturnal/morning O_3 concentrations and higher afternoon peaks than EN, indicating a generally more intense overall O_3 pollution burden associated with LN events. Furthermore, except for autumn where EN and WN

exhibited comparable O_3 levels, WN generally displayed higher O_3 concentrations than EN in other seasons. This indicates that EN exhibited the lowest overall O_3 levels among the three categories, implying that the meteorological conditions triggering EN are relatively the least conducive to overall O_3 accumulation. Overall, the total average O_3 concentrations followed the order: WN (78.02 μg m^{-3}) ≈ LN (77.96 μg m^{-3}) > EN (72.42 μg m^{-3}). The results that WN and LN exhibited comparably high overall levels underscores that prolonged or late-night dynamical intrusions pose a more severe O_3 pollution burden. Moreover, the robustness of these diurnal differences is visually confirmed by the shaded error bands (representing ± 1 standard error of the mean).

9. Results: It is not clear whether the meteorological characterization is based on the 117 days on which NOI events occurred simultaneously across all stations. Does the total in Table S1 sum to 117? The methodological thread connecting event identification, station aggregation, and synoptic classification is not easy to follow. This should be made explicit.

Response 9: Thanks for reviewer's comments. The cross-analysis yielded exactly 171 representative NOI days (when events occurred simultaneously across all stations). We confirm that the specific occurrences listed in Table S1 strictly sum to this total of 171 days, and all subsequent meteorological characterizations were indeed performed based on these 171 days.

Additionally, we have added a dedicated bridging paragraph. This new text outlines the three-step workflow: (1) single-station event identification, (2) multi-station aggregation to extract the 171 simultaneous regional events, and (3) the exclusive use of these 171 days for all subsequent synoptic classifications and meteorological characterizations.

Lines 259-265:

To ensure the utmost methodological clarity, the analytical thread connecting the aforementioned steps is explicitly outlined as follows: First, local NOI events were identified at individual stations based on the absolute increment metric. Second, through the cross-analysis described above, exactly 171 simultaneous regional NOI days were extracted to filter out localized noise. Finally, the subsequent meteorological characterizations and synoptic classifications were strictly executed based exclusively on these 171 representative days.

The Lamb-Jenkinson synoptic circulation classification method was utilized to categorize

weather types for representative NOI days. The categorization results are presented in Table S1 (which sums to exactly 171 days).

10. Discussion and Figures: The discussion of identified weather patterns alongside PBL variations is a welcome addition.

Response 10: We sincerely thank the reviewer for this very encouraging and positive comment.

11. Discussion and Figures: Figure S8 is interesting but needs improvement. A marker or reference point should be added to the left-hand time series column to allow direct comparison with the right-hand column showing trajectory age.

Response 11: Thanks for reviewer's comments. We attempted to add explicit temporal nodes (e.g., 12-h or 24-h age markers) along the 3D pathways. However, because these lines represent the mathematically clustered mean trajectories (averaged from hundreds of individual pathways), the specific discrete hourly nodes cannot be directly extracted or plotted by the clustering software.

To more easily match the specific clusters between the left and right panels relying solely on the color legends, we have added explicit text markers (C1, C2, C3, etc.) next to each corresponding trajectory curve in both the left and right columns.

Figure S8:

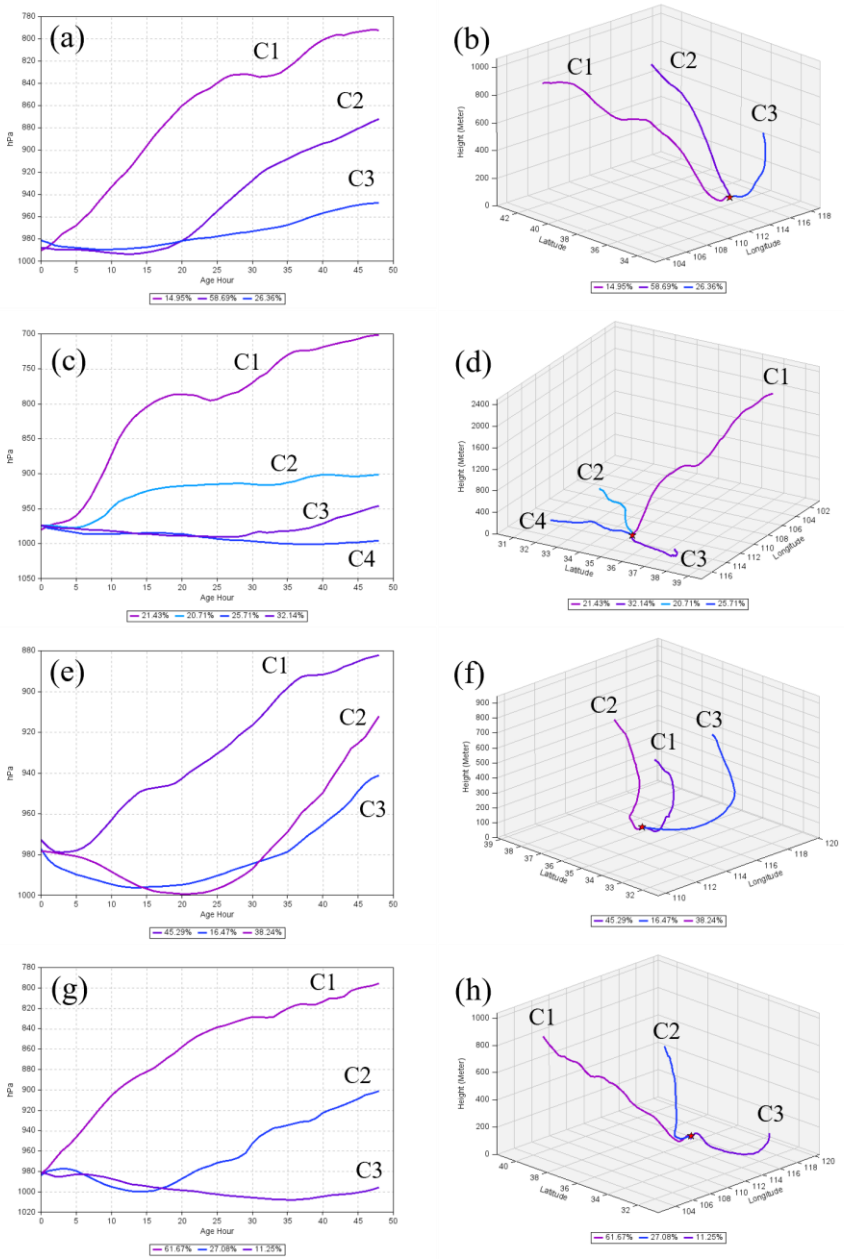


Figure S8: 3D clustered backward trajectories and their corresponding vertical pressure profiles for air masses arriving at Xinxiang under the four weather types. The left column (a), (c), (e), (g) displays the altitude-time cross-sections (represented by atmospheric pressure, hPa) of the trajectory clusters over the 48-hour backward tracking period. The right column (b), (d), (f), (h) illustrates the 3D spatial pathways of these clusters. The four rows from top to bottom correspond to A-type (a, b), C-type (c, d), S-type (e, f), and WNE-type (g, h), respectively. The red star denotes the receptor site (Xinxiang). The percentages in the legends indicate the relative contribution of each trajectory cluster to the total trajectories under that specific weather type. To facilitate a direct and clear comparison between the temporal-altitude profiles (left column) and the spatial pathways (right

column), explicit corresponding markers (e.g., C1, C2, C3) have been added next to each paired trajectory cluster in both panels.

12. Discussion and Figures: Figure 9 is missing units.

Response 12: Thanks for reviewer's comments. We have added the corresponding units to Figure 9.

Figure 9:

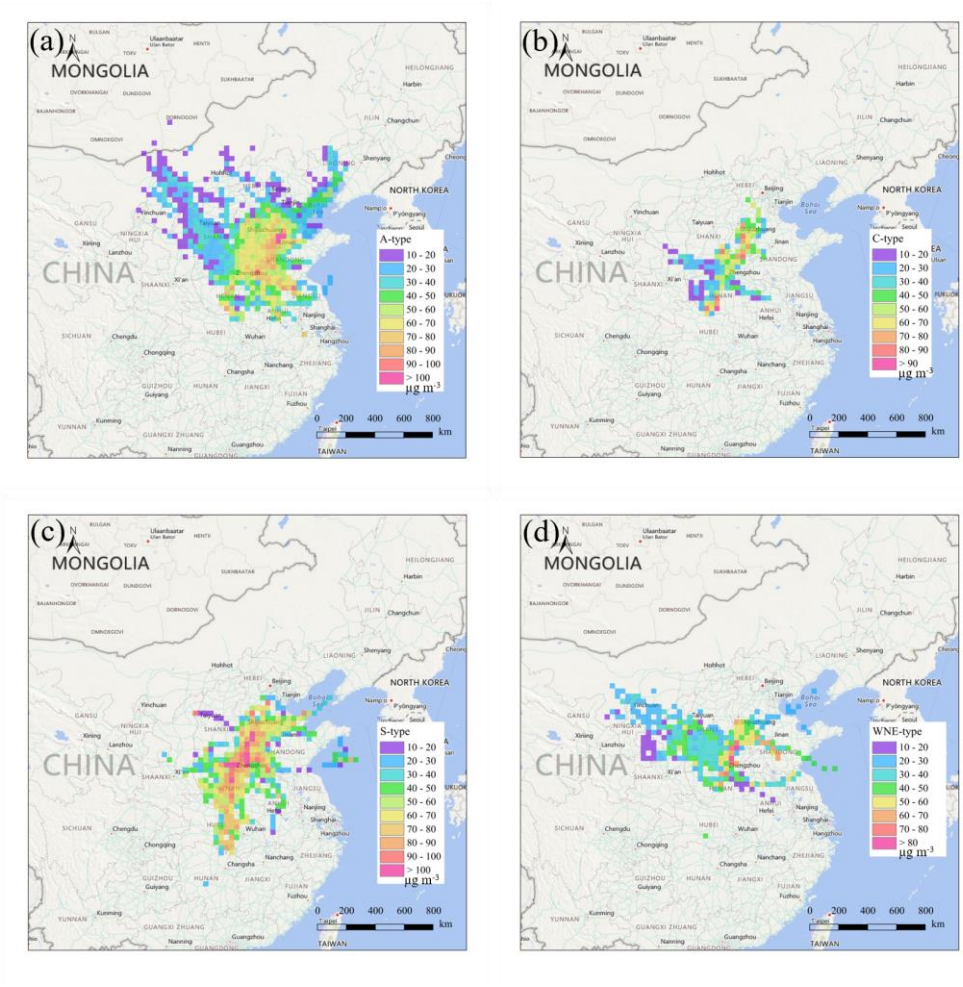


Figure 9: Concentration weighted trajectory (CWT) analysis under different weather types: (a) A-type, (b) C-type, (c) S-type, (d) WNE-type. The base map is provided by Bing Maps.

13. Discussion and Figures: Lines 379–381: The interpretation is not entirely clear. Does this mean that precursors emitted north of the study area entered the atmosphere at altitude and subsequently subsided into the study domain during nocturnal hours?

Response 13: Thanks for reviewer's comments. The physical and chemical sequence we intended

to describe is as follows: The heavy industrial facilities in northern Henan and western Shandong emit abundant precursors. During the daytime, these precursors fuel intense photochemical O_3 production over those areas. After sunset, this formed O_3 is trapped and preserved aloft in the residual layer. When the large-scale weather systems force the air masses to subside during nocturnal hours, these trajectories directly entrain O_3-rich air from the residual layer downwards into the surface of our study domain.

We have revised the text in the manuscript.

Lines 390-396:

When these subsiding trajectories passed over the high O_3 potential source areas in northern Henan and western Shandong (CWT: 90-100 μg m^{-3}; Fig. 9(a)), regions well-documented for their heavy industrial facilities and intense precursor emissions (Lu et al., 2019; Li et al., 2019). During the daytime, these abundant anthropogenic precursors fuel intense photochemical O_3 production over these areas. By nightfall, this locally generated O_3 is preserved aloft within the residual layer. Consequently, when the large-scale subsiding trajectories passed over these regions during nocturnal hours, they directly entrained this O_3-rich air from the residual layer downwards into the surface of our study domain, rather than merely transporting unreacted precursors.

14. Discussion and Figures: Lines 388–391: Similarly, the source attribution here is unclear. Are there not additional source regions contributing via subsidence? The trajectory analysis appears to suggest multiple origins.

Response 14: Thanks for reviewer's comments. We have revised the manuscript to clearly highlight these multiple contributing source origins, as reflected by our trajectory-clustering results.

Lines 402-411:

Influenced by strong geostrophic winds under S-type, southwest airflow pathways dominated (Fig. 8(c)). The CWT analysis (Fig. 9(c)) identified a vast high-value source region (WCWT > 100 μg m^{-3}) encompassing the Central China urban agglomeration to the south, a vast region where intense anthropogenic NO_x and VOCs emissions continuously fuel massive daytime photochemical O_3 accumulation. The vertical profiles (Fig. S8(e)-(f)) confirm that a major portion of this southerly

advection (~45.29%) subsided from the upper boundary layer (~880 hPa). Furthermore, as suggested by the multiple trajectory origins, additional source regions indeed contributed via subsidence. The second-largest cluster (~38.24%) also exhibited subsiding characteristics, descending from ~910 hPa (originating from the northeast). Meanwhile, the remaining cluster (~16.47%) represented lower-altitude horizontal transport originating from the southeast. This comprehensively demonstrates that NOI events under S-type are a superimposed result of multi-source origins, where massive downward subsidence from multiple altitudes couples with regional horizontal advection to collectively elevate the nocturnal O_3 burden.

15. Discussion and Figures: Figure S9: The figure title needs more detail. Units for CAPE are missing. The source of the vertical profiles (ERA5 or MERRA-2?) is not stated.

Response 15: Thanks for reviewer's comments. We have revised both Figure S9 and its corresponding caption.

Figure S9:

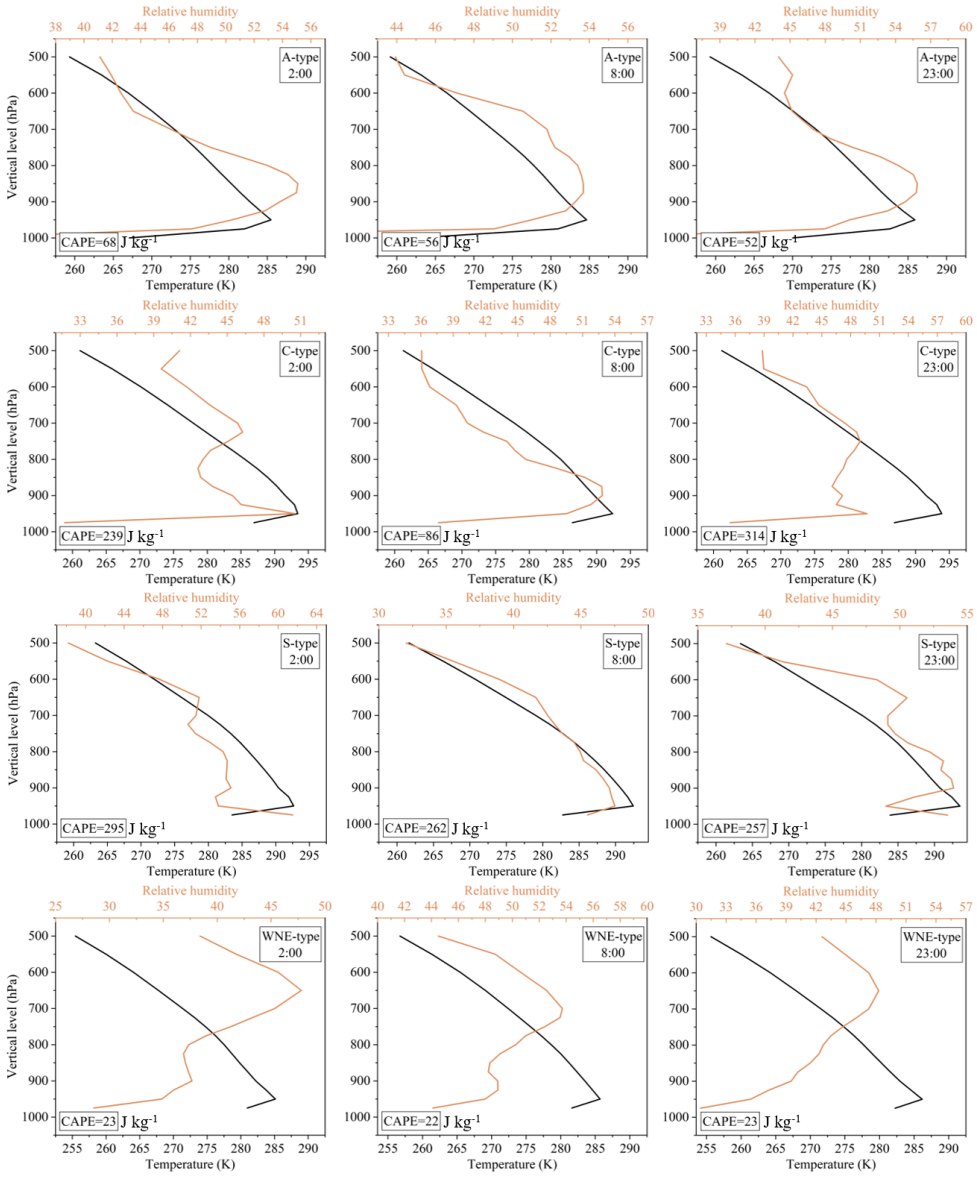


Figure S9: Vertical profiles of temperature (solid black lines, K) and relative humidity (solid orange lines, %) over Xinxiang under the four weather types (A, C, S, and WNE). The three columns from left to right display the vertical atmospheric structure at specific diurnal hours (02:00, 08:00, and 23:00 LT, respectively). The Convective Available Potential Energy (CAPE) values are indicated in the bottom-left corner of each panel, with units in J kg^{-1}. Vertical profiles of temperature and relative humidity are derived from MERRA-2. CAPE data is derived from ERA5.

16. Discussion and Figures: Section 3.4.2: A conceptual diagram of the transport mechanisms identified for each weather type would be highly valuable here — schematic arrows indicating upward and downward motion, interaction with topography, and the proposed transport pathway for

each type. Figure S10 is currently undiscussed in the main text and could be repurposed or adapted to support this conceptual synthesis.

Response 16: Thanks for reviewer's comments. We have revised the former Figure S10 and moved it to the main text as a new main figure (now Figure 12) to serve as the conceptual synthesis. Furthermore, we have added a concluding paragraph at the end of Section 3.4.2.

Figure 12:

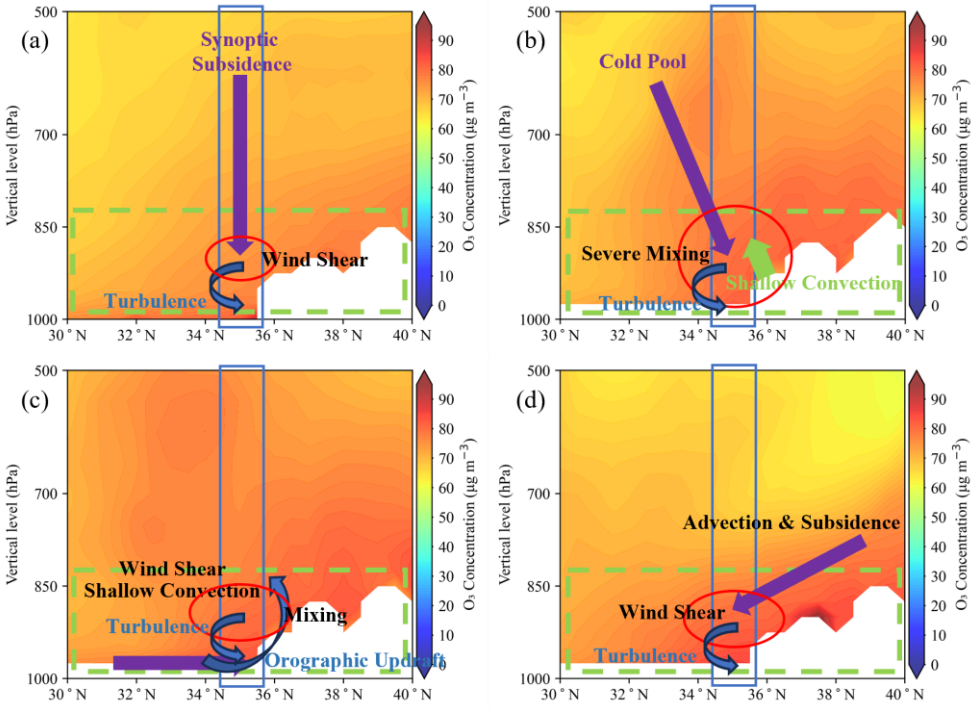


Figure 12: Conceptual diagram synthesizing the transport mechanisms of O_3 under four weather types: (a) A-type, (b) C-type, (c) S-type, (d) WNE-type. The background contours represent the vertical profiles of average O_3 concentrations (green rectangles indicate regions with high O_3 concentration), while blue rectangles denote Xinxiang.

Lines 473-475:

To conceptually synthesize the aforementioned transport mechanisms, we constructed a comprehensive schematic diagram (Fig. 12). This visual summary explicitly illustrates the distinct dynamical pathways for each weather type, highlighting how synoptic forcings and local topography act upon the boundary layer, thereby triggering surface NOI.

17. From a forecasting perspective, what variables or conditions would need to be monitored to anticipate NOI events? Is the proposed approach to track the identified synoptic weather type in combination with friction velocity and PBLH, or do the authors envision a different operational framework? This would be worth addressing briefly in the discussion or conclusions.

Response 17: Thanks for reviewer's comments. We have added a short paragraph in the Conclusions section to briefly discuss the forecasting implication for NOI events. Monitoring synoptic weather-type together with friction velocity and PBLH can provide critical precursors for NOI occurrence.

Lines 509-516:

Overall, our results demonstrate how synoptic-scale circulations and local boundary-layer dynamics couple to cause NOI events. From an operational forecasting perspective, anticipating these events requires a hierarchical monitoring framework. As suggested by our findings, early warning systems should first track the onset of the identified primary synoptic weather types to anticipate large-scale subsidence and advection. Crucially, this macro-scale tracking must be combined with the real-time monitoring of localized boundary-layer metrics, particularly U^* and PBLH, which serve as the direct mechanical triggers for downward transport. This combined approach of monitoring synoptic forcings alongside localized turbulent triggers offers an important physical perspective on the nocturnal O_3 budget and provides actionable guidance for developing precise early warning systems and dynamic pollution control strategies in urban environments.